Precipitation Pattern in the Western Himalayas revealed by Four Datasets

Hong Li[1], Jan Erik Haugen[2], and Chong-Yu Xu[3]

[1]The Norwegian Water Resources and Energy Directorate, Norway
[2]Norwegian Meteorological Institute, Norway
[3]University of Oslo, Norway

Correspondence to: Hong Li (holi@nve.no)

Abstract. Data scarcity is the biggest problem for scientific research related to hydrology and climate studies in the great Himalayas Region. High quality precipitation data are among the most difficult to obtain due to sparse network, cold climate and high heterogeneity in topography. This paper examined four different types of datasets, including interpolated gridded data based on ground observations (IMD, $1° \times 1°$ and APHRODITE, $0.25° \times 0.25°$), reanalysis data (ERA-interim, $0.75° \times 0.75°$) and high resolution simulation by a regional climate model (WRF, $0.15° \times 0.15°$). The study showed in Northern India of the Western Himalayas, the four datasets showed a similar spatial pattern and temporal variation during the period 1981-2007, though the absolute values varied significantly (497-819 mm/year) mainly due to the data source and the methods of data generation. The differences were particularly large in July and August at the windward slopes and the high elevation area. Overall, the datasets showed wetting summer and drying winter, though most of the trends in monthly precipitation were not significant. Trend analysis of summer and winter precipitation at every grids confirmed the changes. Wetting summer will result in more and bigger floods at the downstream areas. Warming and drying winter results in less glaciers accumulation. All the datasets showed consistency through the period and could give a spatial overview of the precipitation in the region. We recommend the APHRODITE dataset and the WRF dataset for hydrological studies for their matched scales with hydrological processes and considerable spatial variation.

1 Introduction

The great Himalayas Region is the largest cryosphere outside the polar areas and is the source of many rivers which supply water to more than 800 million people (Hegdahl et al., 2016; Li et al., 2015b). The population largely depends on rivers for drinking water, hygiene, industry, fishing, and also for agriculture and hydro-power generation, which are the main sectors of local economy (Ménégoz et al., 2013). Therefore, it is very important to understand distribution and changes of precipitation, its impacting factors as well as implications for survival of glaciers.

Precipitation is one of the most important elements in meteorology and hydrology. Besides, precipitation strongly influences human activities. In recent years, with development of space-borne measurements and computing technologies, gridded precipitation datasets have been widely generated and attracted much interest. Compared to traditional ground stations, gridded data

cover a large area, sometimes even the globe, and disclose spatial variability. Additionally, gridded data are usually produced by researchers for scientific purposes and they are free accessible to scientific research. Gridded data have been extensively used, particularly where high quality *in situ* measurements are not available.

Climate change mitigation and adaption are more challenging in economic deficient areas. However, in these area, climate change has more significant impacts on water security. To assess the impacts, the first trouble is lack of high quality data, particularly precipitation, for hydrological studies. Therefore, the first step is to evaluate existing datasets. Here we only selected datasets at a daily time step, which is most often used in hydrological simulations. Additionally, we purposely selected data covering a long period and from various sources, i.e. observations, reanalysis and model simulations.

There have been quite a few studies about precipitation over the Great Himalayas Region (Yatagai et al., 2012; Ménégoz et al., 2013; Palazzi et al., 2013). The available gridded data fall into four types: satellite data, interpolated observation, reanalysis and model simulation. However, all estimations are generally very uncertain due to the complex climate dynamics and local topography, and precipitation rates differ widely among the four types, even among different products of the same type. The satellite data show discrepancies due to platforms and characteristics of sensors. Reflectance from land surface, particularly snow and ice, can cause distinctive biases (Yin et al., 2008). The interpolated observations are usually believed the most reliable. However, great cautions have to be paid when using such data due to inadequacy of interpolating methods and unavoidable inferiors inherited from gauge measurements. For example, underestimation of precipitation could be 58% of annual total precipitation in the cold Alaska region due to wind, wetting loss and trace precipitation (Yang et al., 1998). High resolution climate models provide an alternative perspective and the models are competitive in aspect of high spatio-temporal resolution, identification of precipitation forms (Ménégoz et al., 2013), consistency with other parameters and measurable uncertainties. On the other hand, the simulated data may misrepresent the reality and suffer from inadequacy of boundary and forcing conditions. Reanalysis data are a combination of observations from many sources and dynamic models, but users should be cautious because of continuous changes in observing systems and systematic errors of used models (Dee et al., 2011). Additionally, uncertainties in reanalysis data are difficult to understand and quantify (Dee et al., 2011). The weaknesses of each type are summarized in Table 1.

In this study, four datasets of three types (interpolated observations, reanalysis and model simulations) for a period of 27 years (1981-2007) over the Western Himalayas were used, which is the first of its kind in this region in aspect of number of datasets and data length. The purpose is to compare the datasets and to find their similarity and difference, as well as implications when using them in hydrological studies.

2 Study Area

The study area lies in the northern part of the Indian Himalayan Region (Figure 1). The highest point is 7677 meters above sea level (m a.s.l.), located in the north-eastern region. The low elevation part lies in the south-western region, which adjoins Pakistan. The climate is affected by monsoon and western disturbance. In summer, warm moisture from the Indian Ocean moves northwards and turns west when it hits the high mountains. This interaction brings plenty of precipitation. Precipitation at high mountains falls as snow in winter. Along the course of the moist wind, precipitation decreases from east to west. In winter, the climate is controlled by western turbulence. The mid-latitude low pressure systems bring some snowfall (Ménégoz et al., 2013), but winter is generally quite dry, especially in the coldest region. In this study, seasons are referred based on northern meteorological seasons (spring: March to May; summer: June to August; Autumn: September to November; Winter: December to February).

This area is the headwater of the Indus River and the Ganges River, which are transboundary among China, India, Pakistan and Bangladesh. Additionally, these two rivers have very high hydropower potential. How to explore hydropower is continuously negotiated among the involved countries, which makes the study area very political sensitive.

In the Great Himalayas Region, there are many glaciers and most of them are not regularly monitored. These glaciers are key indicators of regional climate change and water resources. The fates of the glaciers are world-widely concerned by scientific and public communities. Fortunately, the Chhota Shigri glacier in the study area is observed since 1962 and it is representative in term of mass balance for the Western Himalayas glaciers (Azam et al., 2014). Analysis of precipitation data contributes to research of the Chhota Shigri glacier as well as other glaciers in the Western Himalayas.

3 Data

3.1 IMD dataset

The IMD dataset was produced by the India Meteorological Department for the whole India. This dataset temporally covered from 1951 to 2007 and had a spatial resolution of $1° \times 1°$. The data were interpolated from gauge measurements by using the Shepard method (Shepard, 1968). Rajeevan et al. (2006) compared the IMD dataset with the Variability Analysis of Surface Climate Observations (VASClimo) dataset and concluded that the IMD dataset was more accurate in terms of spatial variation. The IMD dataset has been extensively used in climate related research and applications, such as validation of climate models (Bollasina et al., 2011; Wiltshire, 2014) and monsoon variability and predictions (Goswami et al., 2006).

The number of used stations varied during the period as well as across the region. During this study period, the average number of stations per grid point was 2.99 ranging from 0.2 to 4.4 (Rajeevan et al., 2006). Spatially, more stations were used

in the central south; less stations near the borders of India and in the northern part. No station measurements were available near the latitude of 35.5°N and its north.

3.2 APHRODITE dataset

The APHRODITE (Asian Precipitation—Highly Resolved Observational Data Integration Towards Evaluation of Water Resources) dataset was interpolated by the Sphere map method based on data collected at 5,000–12,000 stations (Yatagai et al., 2012). The interpolated parameter was the precipitation anomaly or ratio, instead of the precipitation amount (Yatagai et al., 2012). Elevation corrections were considered by a weighting function, which was based on the angular distance with considering topography (Yatagai et al., 2012). The dataset covered Asia over the period of 1951-2007. Different versions of the APHRODITE dataset have been used to determine of Asian monsoon precipitation change, hydrological modelling (Pechlivanidis and Arheimer, 2015; Xu et al., 2016), verification of high-resolution model simulations and satellite precipitation estimates (Kamiguchi et al., 2010). In this research, we used the latest version (V1101) for monsoon Asia at a spatial resolution of 0.25°×0.25° (Dimri et al., 2013). The APHRODITE dataset involved the largest number of gauge observations among interpolated products, and is believed to be one of the most realistic precipitation datasets for Asia (Ménégoz et al., 2013).

3.3 ERA-interim dataset

The ERA-interim dataset is the precipitation product of the ERA-Interim (Dee et al., 2011), which is a spatially and temporally complete data set of multiple climate variables at high spatial and temporal resolution. The data we used here were on a Gaussian grid (with a resolution of 0.7×0.7° at the Equator) with a 3-hour time resolution, and aggregated to daily time step. The ERA-Interim is global atmospheric reanalysis produced by the ECMWF (European Centre for Medium-Range Weather Forecasts) [1]. The dataset dates back to 1979 and is updated with approximately 1 month delay from real-time. The data assimilation system is based on a 2006 release of the IFS (Cy31r2) (Dee et al., 2011) and precipitation is adjusted based on Global Precipitation Climatology Project v2.1 (Adler et al., 2003), which is another interpolated observation product, before release. This dataset has been widely used as boundary and forcing conditions for regional climate models (Dimri et al., 2013; Katragkou et al., 2015).

3.4 WRF dataset

The WRF dataset was generated by using a regional climate model, the Weather Research & Forecasting Model (v3.7.1). The climate model is a limited-area, non-hydrostatic, primitive-equation model with multiple options for various physical parameterization schemes. The model has been used in climate simulation in Asia and other areas (Maussion et al., 2011) and (Li et al., 2016). It is not easy to determine an optimized selection of parameterization scheme in the Great Himalayas Region. Here we carefully selected the parameterization scheme with consideration of published studies, such as Maussion et al. (2011); Li et al. (2016). The main setting was shown in Table 2 and the whole setting was supplementary.

---

[1]The next generation reanalysis, ERA5, featuring a higher horizontal resolution (~31 km) and a 10-member ensemble approach for uncertainty estimates, was released by the end of 2017. See e.g. http://www.ecmwf.int/en/newsletter/147/news/era5-reanalysis-production

3.5 Discharge

Three discharge series were selected to cross validate water balance. They were respectively Pandoh (downstream), Bhuntar (middle stream) and Manali (upstream). The catchments are located in the Beas basin, which is a main tributary of the Indus River in Northern India (Figure A1). The catchments are nested from upstream to downstream. The purpose is to reflect precipitation data at various elevations within a hydrological scale. Runoff is considerably influenced from glacier melting (Li et al., 2015a). According to the 0.5 km MODIS-based Global Land Cover Climatology by the USGS Land Cover Institute (https://landcover.usgs.gov/global_climatology.php), coverage of snow and ice is 16% in the Pandoh catchment, 24% in the Bhuntar catchment and 21% in the Manali catchment. The discharge data have been manually quality controlled and missing data were filled by discharge anomaly.

3.6 Evaporation

The MODIS Global Evapotranspiration Project (MOD16) (http://www.ntsg.umt.edu/project/modis/mod16.php) was selected to reveal actual evaporation. The MODIS project started in 2000, and had a short overlap period with the study period. Additionally, part of the catchments is covered by permanent snow and ice and the sensors could not work well on this type surface. Therefore, we used annual mean amounts of 2000 to 2013 to reduce uncertainties. The missing ratios of annual mean actual evaporation are 22% for the Pandoh catchment, 32% for the Bhuntar catchment and 31% for the Manali catchment.

4 Results

4.1 Spatial variations

The four datasets showed similar spatial pattern of annual precipitation (Figure 2). The highest precipitation was located at the foothill of the mountains and stretched from southeast to northwest. Visually, the high precipitation belt (the foothills of the mountains and the southeastern corner) was most clearly shown by the WRF dataset. The spatial variability increased from the IMD dataset to the WRF dataset. Their coefficients of variation were respectively 0.5 for the IMD data, 0.6 for the ERA-interim data, 0.7 for the APHRODITE data and 1.1 for the WRF data. The density curves (Figure 3) showed the variabilities more clearly.

Both the IMD and APHRODITE datasets originated from station observations. However, the APHRODITE dataset showed a rain belt at the mountains' foothills much better due to its finner spatial resolution. Additionally, the APHRODITE dataset showed much lower estimations (less than 300 mm/year) at the north-eastern corner. This area was quite high, with mean elevation at 4650 m a.s.l. and elevation ranging from 906 to 7677 m a.s.l. The temperature was -2.35 °C of annual mean and as low as -16.81 °C in January (AphroTemp, Yatagai et al., 2012). The reason for this low precipitation area was the APHRODITE dataset basing on more stations, particularly also observations from Nepal, Bhutan and China (Yatagai et al., 2012). These stations had under-catch problems, which means rain gauges could only catch part of snowfall due to wind and disturbance.

In contrast, the IMD dataset used only the stations at the low valley area of India and extended to the border by interpolation (Rajeevan et al., 2006). Eventually, the APHRODITE dataset had the lowest annual amount, only 61% of the IMD dataset.

The ERA-interim and WRF datasets were products with different dynamical models, whereas the ERA-interim precipitation dataset was adjusted to the GPCC monthly precipitation dataset. The ERA-interim data and the WRF data were similar in terms of annual total amount (ERA-interim: 718 mm/year, WRF: 688 mm/year) and spatial pattern, partially due to the fact that in this area the observations that were assimilated into the data assimilation system were sparse and unevenly distributed. The WRF data were more realistic than the ERA-interim data due to finner spatial resolution, especially in complex topography areas (Ménégoz et al., 2013; Dimri et al., 2013). Spatial resolution of regional climate models is definitely important in the mountainous areas (Ménégoz et al., 2013), but it is quite computing intensive and time expensive. Most simulations were at 50 km for years (Polanski et al., 2010; Maussion et al., 2011; Dimri and Niyogi, 2013; Dimri et al., 2013) or fine resolutions for months (Ménégoz et al., 2013). Our simulations at 16 km spatial resolution over 29 years was rarely reported.

The summer monsoon and winter monsoon respectively bring the precipitation in summer and winter. Here we selected two months (highest and lowest amount) in each season, clearly show patterns against elevation. As shown in Figure 4, precipitation in both seasons showed the similar pattern – "curved sword". For instance, the summer precipitation increased with the elevation at the low area (100 - 800 m a.s.l). However, at approximately 700 m a.s.l, the range of precipitation became large. It resembled the grip part of a sword. At 2500 m a.s.l, the precipitation was at a high level (250 mm/month). At high area, the precipitation decreased with elevation. This curved sword pattern was more clear in summer than in winter and there was a large variation between datasets. It should be noted here that the presented elevation was slightly lower than the actual values due to spatial interpolation.

The effects of location and topography were shown in Figure 5. The summer monsoon came from the southeast and the precipitation decreased along the path. Over the high flat plateau, precipitation decreased with latitude since the strength of monsoon decreased with distance from its source. As the monsoon got closer to the mountains, precipitation started to increase. As the air parcel lifted to high elevation, climate got dry and cold. The winter monsoon traveled from the northwest (Dimri and Niyogi, 2013) and it was cold and dry. Therefore, precipitation occurred mainly along the up-slope. The magnitude was also small and decreased along the path of winter monsoon. The highest precipitation occurred in the windward of the up-slope region, but it was 0.5 or 1.5 degree (around 55-110 km) far away from the mountains in summer. Bookhagen and Burbank (2006) analyzed a decade of TRMM data and also found the highest annual precipitation was offset by a few 10s of km south of either high topography or relief. This offset had been found only over tall and broad mountain regions rather than narrow mountain peaks (Dimri and Niyogi, 2013).

The differences among the datasets were more obvious at high elevation. The WRF dataset gave much more precipitation in summer and where elevation was below 3000 m a.s.l. The WRF model was ever reported moist biased in summer (Srinivas

et al., 2013; Li et al., 2016). It was often cited as orographic bias which described as strong over-prediction of precipitation rates along windward slopes while predicted snowfall lay under measured values along leeward slopes (Maussion et al., 2011). However, it was not fair to interpret purely as model errors and ignore inaccuracy in measurements. Discharge measurements are generally more qualified than precipitation in the snow and ice dominated area (Henn et al., 2015; Kretzschmar et al., 2016).

5   Therefore, the quality of runoff simulation can infer by the forcing precipitation data. Li et al. (2016) used the WRF-Hydro (v3.5.1) modeling system in the Beas Basin, and they found that the distribution of simulated daily discharge values agreed well with observations, which reversely confirmed the precipitation simulations.

4.2 Temporal variations and changes

The inter-annual patterns were very similar as indicated by high correlations between pairs of datasets, shown in Table 3. The
10   correlation between the IMD and APHRODITE datasets was the highest, reaching 0.91. The WRF dataset had low correlation with all other datasets. Spatially, the four datasets showed a similar seasonal distribution, and the WRF dataset had the highest variability (Figure 6). The intra-annual cycle was also similar as shown in Figure 7. The WRF and APHRODITE datasets had respectively the highest and lowest precipitation in summer.

15   To look at changes over time, we selected the Theil-Sen median method to calculate trend due to its robustness and the non-parametric Mann-Kendall test for the significance test. The trend analysis and significance test were done for areal mean of each month (Figure 7), and every individual grid for summer (Figure 8 and 9) and winter (Figure 11 and 10). The figures showed increase in summer precipitation and decrease in winter precipitation, although both increase and decrease existed in each dataset. Three of the areal mean trends (May by the WRF dataset; June by the IMD and ERA-interim datasets) were
20   statistically significant at the 95% confidence level. The spatial distribution of trends in summer precipitation varied a lot. Most decreasing trends of winter precipitation occurred at the northern part. Approximately 10% grids were significant at the 10% confidence level.

It is difficult to conclude why the Northern India of the Western Himalayas showed an increase in summer precipitation.
25   However, Bollasina et al. (2011) found the same increasing monsoon precipitation in the Northern India, whereas decreasing in the Central Asia. They used a series of climate model experiments, and concluded that such pattern was a robust outcome of a slowdown of the tropical meridional overturning circulation, which could be attributed mainly to human-influenced aerosol emissions. The trends will continue and become more significant with time if greenhouse gas emission continues as usual. Such trends would lead to strong negative mass balance conditions of glaciers, which was discussed in the next section.

30 5   Discussions

5.1   Comparison with runoff data

The annual actual evaporation from MODIS data was 614 mm/year at the Pandoh catchment, 639 mm/year at the Bhuntar catchment and 649 mm/year at the Manali catchment. The values were too high compared with 64mm/year at the Pandoh catchment for the period from 1990 to 2004 calculated by Kumar et al. (2007) using potential evaporation, mean and maxim temperature. The Pandoh catchement covered the lower and middle parts, and should have the highest evaporation due to warm

5 climate among three catchments. The MODIS data were not qualified at the catchments and at small catchment scales for the study period.

The precipitation and runoff relationship was shown in Figure 12 as accumulation of monthly precipitation and runoff. Though the lines had different slopes, but they shared very similar linear relationships and they were consistent in terms of temporal

10 changes and errors were systematic within each dataset. Runoff is generally less than precipitation due to evaporation loss. However, runoff could possibly exceed precipitation at glacierised catchment due to glacier melting. Runoff was most more than precipitation in the Manali catchment. In the Bhuntar catchment, only the ERA-interim data showed less runoff than precipitation. All datasets show less runoff than precipitation in the Pandoh catchment. Precipitation was definitely underestimated at higher elevation area, especially in the Manali catchment. Azam et al. (2014) reconstructed annual mass balance of Chhota

15 Shigri glacier since 1969. The Chhota Shigri glacier lies in the Western Himalaya, India and it is representative in terms of mass balance for the Western Himalayas glaciers (Azam et al., 2014). The mass loss rates were 0.36±0.36 for 1969 to 1985 and 0.57±0.36 m water equivalent per year (m w.e.a^{-1}) for 2001 to 2015. The runoff contributed from glacier melting was only 3306 mm within 29 years with assumptions of 20% glacier coverage and -0.57 m w.e.a^{-1}.

5.2 Implications for glaciers

20 Temperature in combination with precipitation controls survival of glaciers. Therefore, we also looked at changes in temperature by comparing the temperature results by the same simulation of the WRF precipitation dataset for the first and last five years, namely 1981-1985 and 2003-2007. We skipped the trend analysis and significance test, because it is already well known that temperature is increasing fast in the Great Himalayas Region since 1980s (Ren et al., 2017). Temperature is generally better measured and more certain and no need to go through many datasets. Here we were particularly interested in temperature

25 at the equilibrium line altitude (ELA). As shown in Figure 13, the WRF model was able to reproduce the dry and wet lapse rates. Between the two five-years, temperature increased 0.91 °C in winter and 0.26 °C in summer. Such changes led to the elevation of freezing point (0 °C) moving up 125 m in winter and 32 m in summer. As shown in Section 4.2, precipitation overall decreased in winter. Combined with increasing temperature, it was an unfavourable condition for the glaciers: less accumulation and faster melting. Moreover, the area between 4900 m a.s.l., which was the equilibrium line altitude (ELA) of

30 the Chhota Shigri glacier (see Azam et al., 2012, Figure 2), and 5200 m a.s.l. was large. Therefore, as the climate got warmer, the ELA would further move up. Such a nonlinear characteristic of elevation distribution resulted in a potential large reduction in the accumulation area and small storage buffer of permanent snow and ice.

6 Conclusions

Data scarcity is the biggest problem for hydrological research in the Great Himalayas Region. High quality precipitation data are among the most difficult to obtain due to the sparse network, cold climate and high heterogeneity in topography. This paper investigated the spatial and temporal pattern of precipitation in this region based on different types of datasets, including interpolated gridded data based on ground observations (IMD, $1° \times 1°$ and APHRODITE, $0.25° \times 0.25°$), reanalysis data (ERA-interim, $0.75° \times 0.75°$) and high resolution simulation by a regional climate model (WRF, $0.15° \times 0.15°$) in Northern India of the Western Himalayas during the period 1981-2007.

The four datasets were similar in terms of spatial pattern and temporal variation and changes, though the absolute values varied a lot (497-819 mm/year) due to the data source and the methods of data generation. The differences were particularly large in July and August and at the windward slopes and the high elevation areas. The datasets revealed that summer was becoming wetter and winter was becoming drier, though most of the trends were not statistically significant. Wetting summer resulted in more and bigger floods at the downstream areas. Warming and drying winter resulted in less glaciers accumulation. The four datasets were able to give a good overview of spatial pattern and temporal changes. The APHRODITE and WRF datasets are recommended for hydrological studies due to good scales and spatial variations. However, careful local correction is definitely required.

Acknowledgements. This study is funded by the Research Council of Norway through the research program NORKLIMA under grant the project 216546. We thank India Meteorological Department and Sonia Grover at Water Resources Division at TERI (India), European Centre for Medium-Range Weather Forecasts and the APHRODITE (http://www.chikyu.ac.jp/precip/english/products.html) and the research program JOINTINDNOR under grant the project 203867 for provision of data. We thank Oskar Landgren at the Norwegian Meteorological Institute for assistance in modelling and data analysis as well as review of the manuscript. The model simulation was done when the first author when she worked at the Norwegian Meteorological Institute.

Conflict of Interest

No conflict of interest.

7 Code availability

8 Data availability

The ERA-interim and APRODITE data are available from the data provider sites. The WRF data are available via https://archive.norstore.no/pages/public/about.jsf.

Author contributions. Hong Li: model simulation, data analysis and draft. Jan Erik Haugen: model simulation and results analysis. Chongyu Xu: draft review and manuscript modification.

References

Adler, R. F., Huffman, G. J., Chang, A., Ferraro, R., Xie, P.-P., Janowiak, J., Rudolf, B., Schneider, U., Curtis, S., Bolvin, D., Gruber, A., Susskind, J., Arkin, P., and Nelkin, E.: The Version-2 Global Precipitation Climatology Project (GPCP) Monthly Precipitation Analysis (1979–Present), American Meteorological Society, 4, 1147–1167, 2003.

Azam, M. F., Wagon, P., Ramanathan, A., Vincent, C., Sharma, P., Arnaud, Y., Linda, A., Pottakkal, J. G., Chevallier, P., Singh, V. B., and Berthier, E.: From balance to imbalance: a shift in the dynamic behaviour of Chhota Shigri glacier, western Himalaya, India, Journal of Glaciology, 58, 315–324, 2012.

Azam, M. F., Wagnon, P., Vincent, C., Ramanathan, A., Linda, A., and Singh, V. B.: Reconstruction of the annual mass balance of Chhota Shigri glacier, Western Himalaya, India, since 1969, Annals of Glaciology, 55, 69–80, 2014.

Bollasina, M. A., Ming, Y., and Ramaswamy, V.: Anthropogenic Aerosols and the Weakening of the South Asian Summer Monsoon, Science, 2011.

Bookhagen, B. and Burbank, D. W.: Topography, relief, and TRMM-derived rainfall variations along the Himalaya, Geophysical Research Letters, 33, L08 405, 2006.

Dee, D. P., Uppala, S. M., Simmons, A. J., Berrisford, P., Poli, P., Kobayashi, S., Andrae, U., Balmaseda, M. A., Balsamo, G., Bauer, P., Bechtold, P., Beljaars, A. C. M., van de Berg, L., Bidlot, J., Bormann, N., Delsol, C., Dragani, R., Fuentes, M., Geer, A. J., Haimberger, L., Healy, S. B., Hersbach, H., Hólm, E. V., Isaksen, L., Kållberg, P., Köhler, M., Matricardi, M., McNally, A. P., Monge-Sanz, B. M., Morcrette, J.-J., Park, B.-K., Peubey, C., de Rosnay, P., Tavolato, C., Thépaut, J.-N., and Vitart, F.: The ERA-Interim reanalysis: configuration and performance of the data assimilation system, Quarterly Journal of the Royal Meteorological Society, 137, 553–597, 2011.

Dimri, A. P. and Niyogi, D.: Regional climate model application at subgrid scale on Indian winter monsoon over the western Himalayas, International Journal of Climatology, 33, 2185–2205, 2013.

Dimri, A. P., Yasunari, T., Wiltshire, A., Kumar, P., Mathison, C., Ridley, J., and Jacob, D.: Application of regional climate models to the Indian winter monsoon over the western Himalayas., The Science of the total environment, 468-469 Su, S36–47, 2013.

Goswami, B. N., Venugopal, V., Sengupta, D., Madhusoodanan, M. S., and Xavier, P. K.: Increasing Trend of Extreme Rain Events Over India in a Warming Environment, Science, 2006.

Hegdahl, T. J., Tallaksen, L. M., Engeland, K., Burkhart, J. F., and Xu, C.-Y.: Discharge sensitivity to snowmelt parameterization: a case study for Upper Beas basin in Himachal Pradesh, India, 2016.

Henn, B., Clark, M. P., Kavetski, D., and Lundquist, J. D.: Estimating mountain basin-mean precipitation from streamflow using Bayesian inference, Water Resources Research, 51, 8012–8033, 2015.

Kamiguchi, K., Arakawa, O., Kitoh, A., Yatagai, A., Hamada, A., and Yasutomi, N.: Development of APHRO_JP, the first Japanese high-resolution daily precipitation product for more than 100 years, Hydrological Research Letters, 4, 60–64, 2010.

Katragkou, E., García-Díez, M., Vautard, R., Sobolowski, S., Zanis, P., Alexandri, G., Cardoso, R. M., Colette, A., Fernandez, J., Gobiet, A., Goergen, K., Karacostas, T., Knist, S., Mayer, S., Soares, P. M. M., Pytharoulis, I., Tegoulias, I., Tsikerdekis, A., and Jacob, D.: Regional climate hindcast simulations within EURO-CORDEX: evaluation of a WRF multi-physics ensemble, Geoscientific Model Development, 8, 603–618, 2015.

Kretzschmar, A., Tych, W., Chappell, N. A., and Beven, K. J.: Reversing hydrology: quantifying the temporal aggregation effect of catchment rainfall estimation using sub-hourly data, Hydrology Research, 2016.

Kumar, V., Singh, P., and Singh, V.: Snow and glacier melt contribution in the Beas River at Pandoh Dam, Himachal Pradesh, India, Hydrological Sciences Journal, 52, 376–388, 2007.

Li, H., Beldring, S., Xu, C.-Y., Huss, M., Melvold, K., and Jain, S. K.: Integrating a glacier retreat model into a hydrological model – Case studies of three glacierised catchments in Norway and Himalayan region, Journal of Hydrology, 527, 656–667, 2015a.

5   Li, H., Xu, C.-Y., Beldring, S., Tallaksen, L., and Jain, S. K.: Water Resources under Climate Change of Himalayan Basins, Water Resources Management, 2015b.

Li, L., Gochis, D. J., Sobolowski, S., and Mesquita, M. d. S.: Evaluating the present annual water budget of a Himalayan headwater river basin using a high-resolution atmosphere-hydrology model, in: EGU General Assembly Conference Abstracts, vol. 18, 2016.

Maussion, F., Scherer, D., Finkelnburg, R., Richters, J., Yang, W., and Yao, T.: WRF simulation of a precipitation event over the Tibetan
10   Plateau, China – an assessment using remote sensing and ground observations, Hydrology and Earth System Sciences, 15, 1795–1817, 2011.

Ménégoz, M., Gallée, H., and Jacobi, H. W.: Precipitation and snow cover in the Himalaya: from reanalysis to regional climate simulations, Hydrology and Earth System Sciences, 17, 3921–3936, 2013.

Palazzi, E., von Hardenberg, J., and Provenzale, A.: Precipitation in the Hindu-Kush Karakoram Himalaya: Observations and future scenarios,
15   Journal of Geophysical Research: Atmospheres, 118, 85–100, 2013.

Pechlivanidis, I. G. and Arheimer, B.: Large-scale hydrological modelling by using modified PUB recommendations: the India-HYPE case, Hydrology and Earth System Sciences, 19, 4559–4579, 2015.

Polanski, S., Rinke, A., and Dethloff, K.: Validation of the HIRHAM-simulated Indian summer monsoon circulation, Advances in Meteorology, 2010.

20   Rajeevan, M., Bhate, J., Kale, J. D., and Lal, B.: High resolution daily gridded rainfall data for the Indian region: Analysis of break and active monsoon spells, Current Science, 2006.

Ren, Y.-Y., Ren, G.-Y., Sun, X.-B., Shrestha, A. B., You, Q.-L., Zhan, Y.-J., Rajbhandari, R., Zhang, P.-F., and Wen, K.-M.: Observed changes in surface air temperature and precipitation in the Hindu Kush Himalayan region over the last 100-plus years, Advances in Climate Change Research, 8, 148–156, 2017.

25   Shepard, D.: A two-dimensional interpolation function for irregularly-spaced data, in: Proceedings of the 1968 23rd ACM national conference, pp. 517–524, 1968.

Srinivas, C. V., Hariprasad, D., Bhaskar Rao, D. V., Anjaneyulu, Y., Baskaran, R., and Venkatraman, B.: Simulation of the Indian summer monsoon regional climate using advanced research WRF model, International Journal of Climatology, 33, 1195–1210, 2013.

Wiltshire, A. J.: Climate change implications for the glaciers of the Hindu Kush, Karakoram and Himalayan region, The Cryosphere, 8,
30   941–958, 2014.

Xu, H., Xu, C.-Y., Chen, S., and Chen, H.: Similarity and difference of global reanalysis datasets (WFD and APHRODITE) in driving lumped and distributed hydrological models in a humid region of China, Journal of Hydrology, 542, 343–356, 2016.

Yang, D., Goodison, B. E., Ishida, S., and Benson, C. S.: Adjustment of daily precipitation data at 10 climate stations in Alaska: Application of World Meteorological Organization intercomparison results, Water Resources Research, 34, 241–256, 1998.

35   Yatagai, A., Kamiguchi, K., Arakawa, O., Hamada, A., Yasutomi, N., and Kitoh, A.: APHRODITE: Constructing a Long-Term Daily Gridded Precipitation Dataset for Asia Based on a Dense Network of Rain Gauges, Bulletin of the American Meteorological Society, 93, 1401–1415, 2012.

Yin, Z.-Y., Zhang, X., Liu, X., Colella, M., and Chen, X.: An Assessment of the Biases of Satellite Rainfall Estimates over the Tibetan Plateau and Correction Methods Based on Topographic Analysis, Journal of Hydrometeorology, 9, 301–326, 2008.

Figures
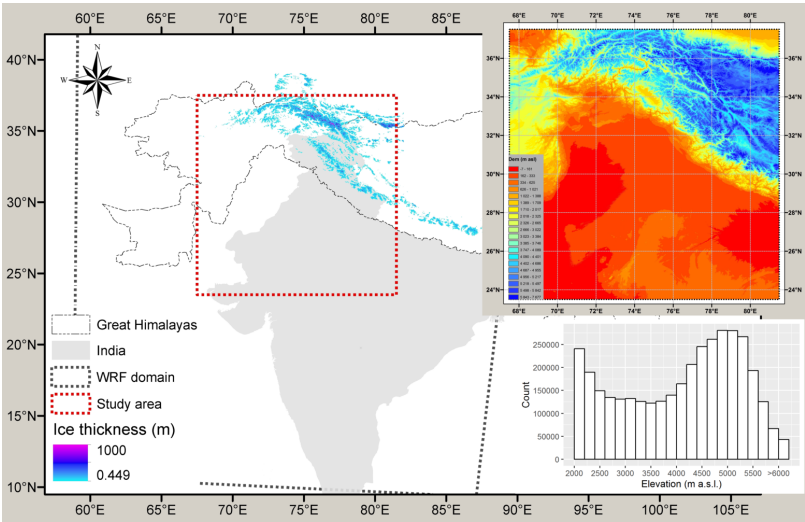
Figure 1. The location and elevation of the study area. The elevation source is HydroSHEDS (http://hydrosheds.org/).
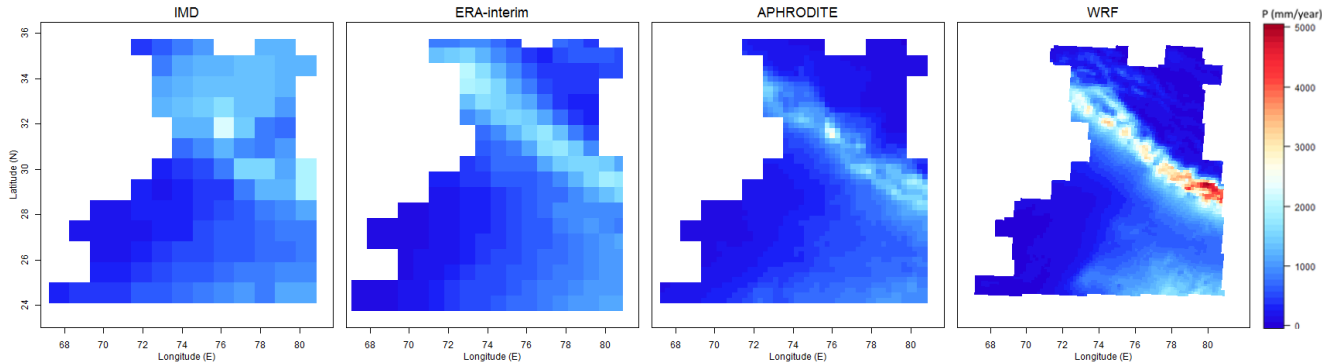
Figure 2. Annual precipitation.
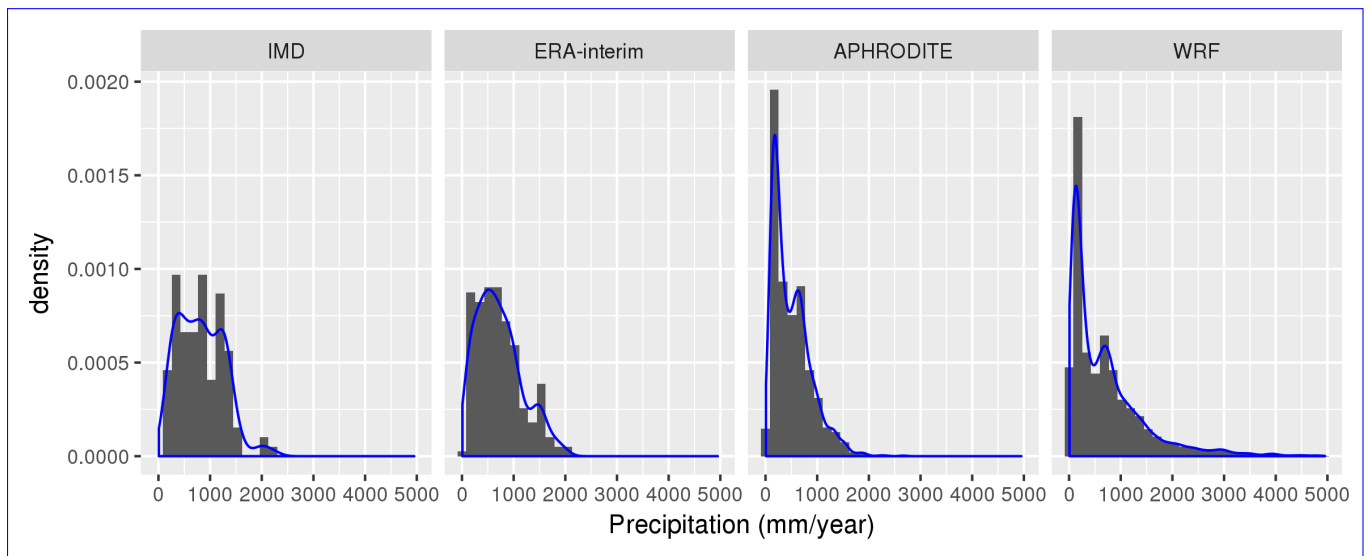
Figure 3. Density plot of annual mean precipitation.
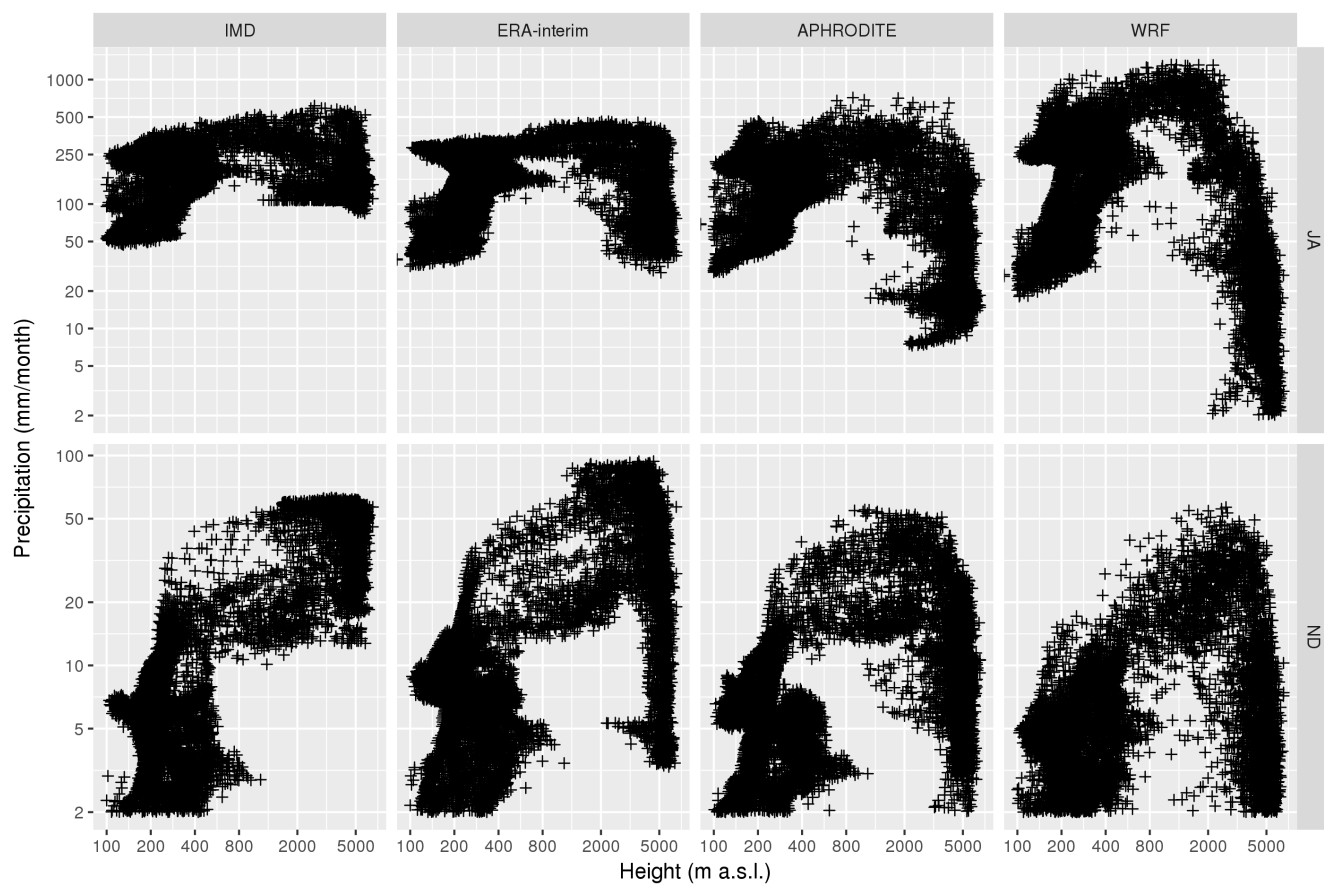
Figure 4. JA (July, August – top) and ND (November, December – bottom) precipitation against elevation. Note that axes are not linear.
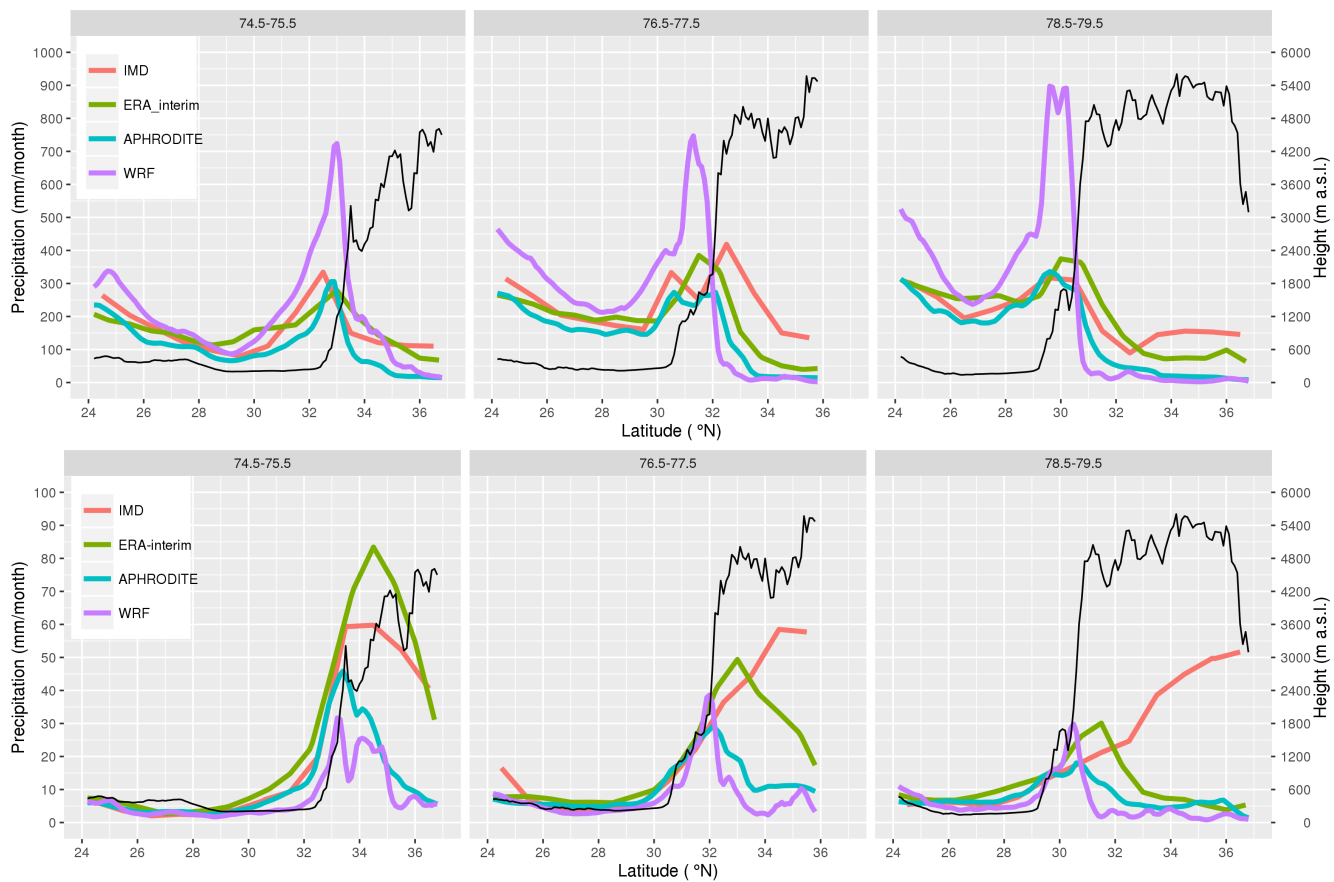
Figure 5. JA (July, August – top) and ND (November, December – bottom) precipitation elevation (mean in the selected longitude box) from west to east.
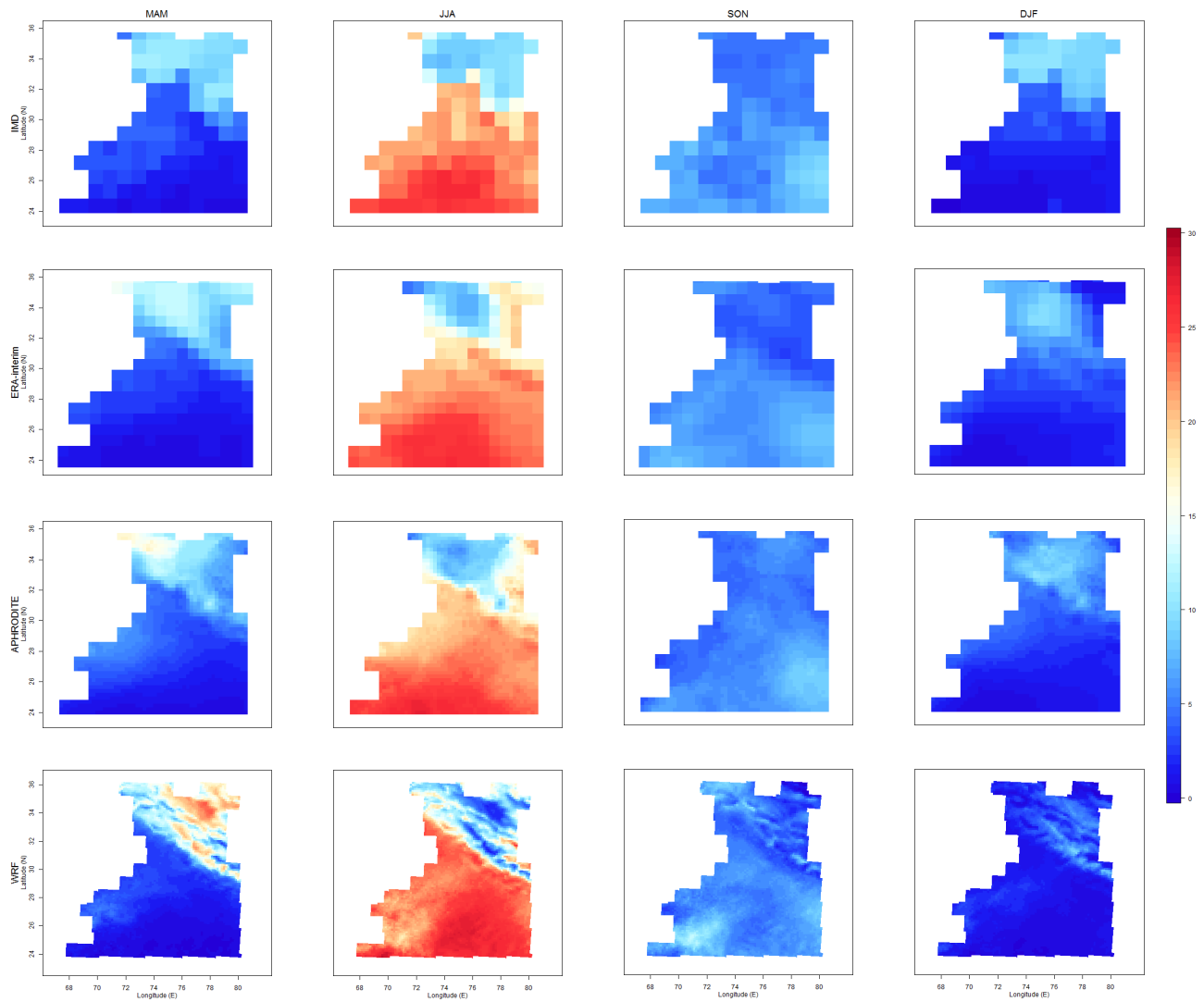
Figure 6. Seasonal contributions (%) to annual precipitation.
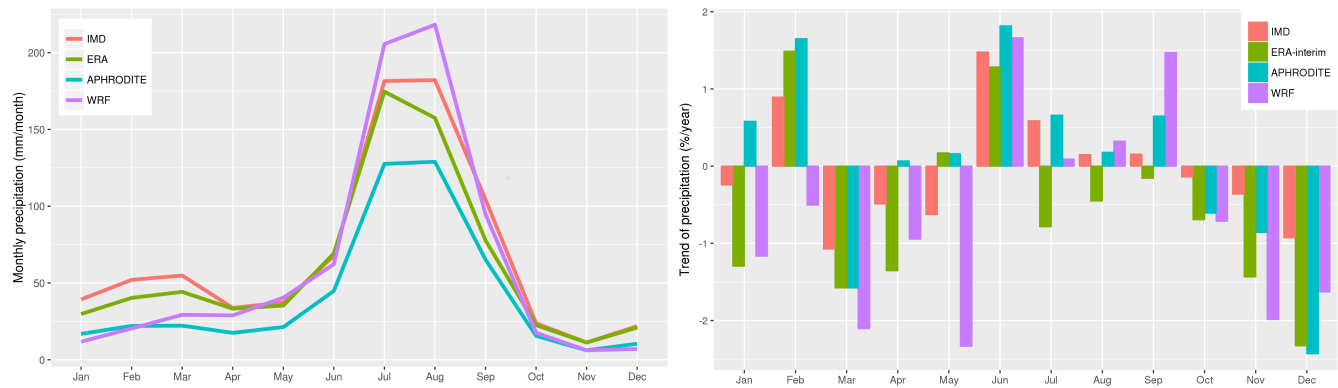
Figure 7. Monthly precipitation (left) and the trend during 1981-2007 (right).
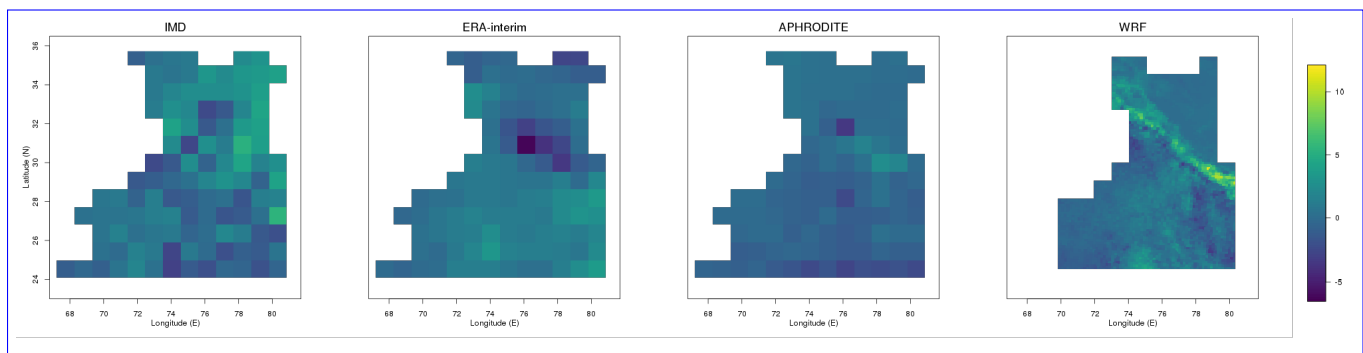
Figure 8. Trend (mm/month/year) of summer precipitation.
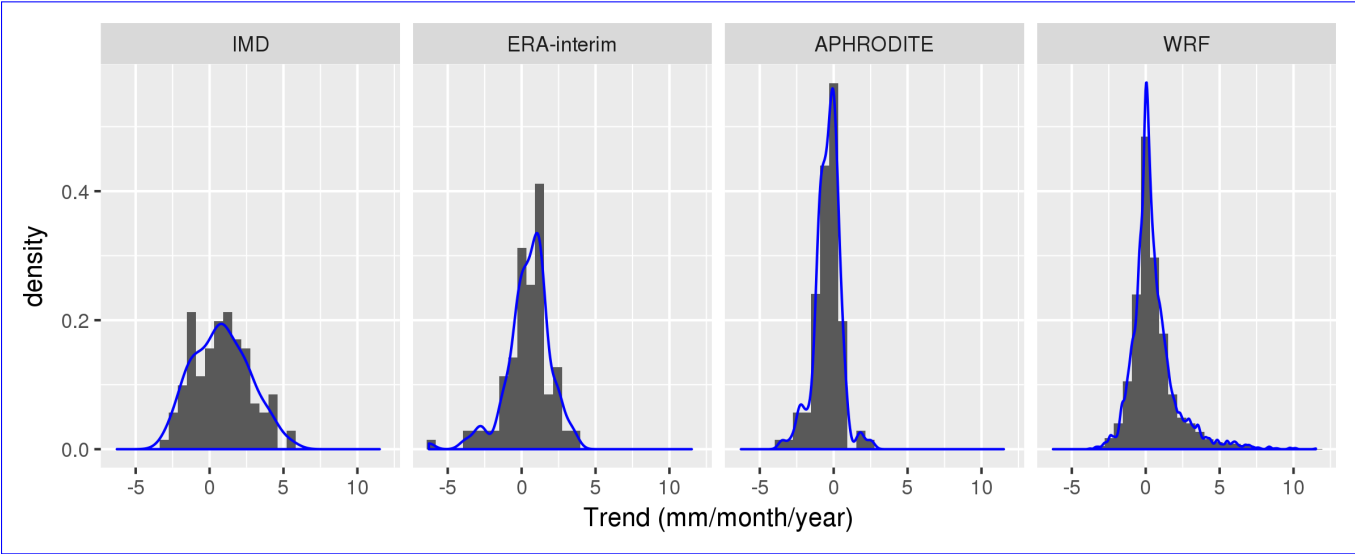
Figure 9. Density plot of trends (mm/month/year) of summer precipitation.
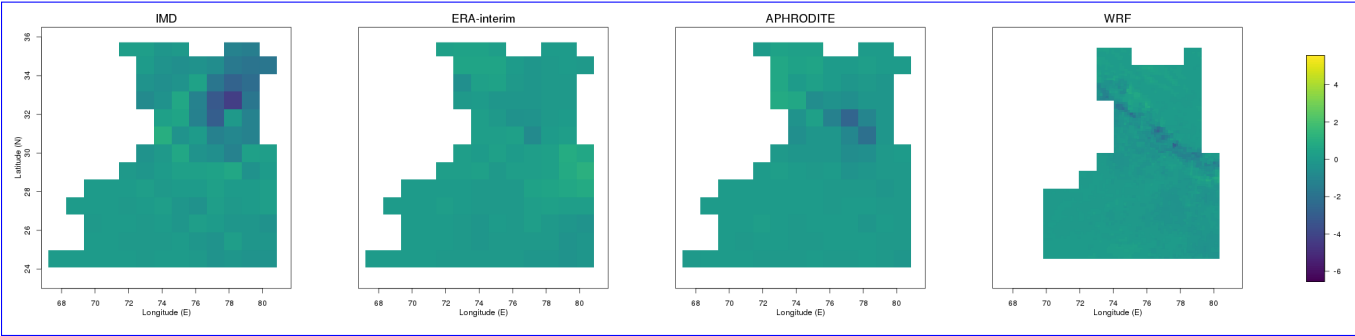
Figure 10. Density plot of trends (mm/month/year) of winter precipitation.
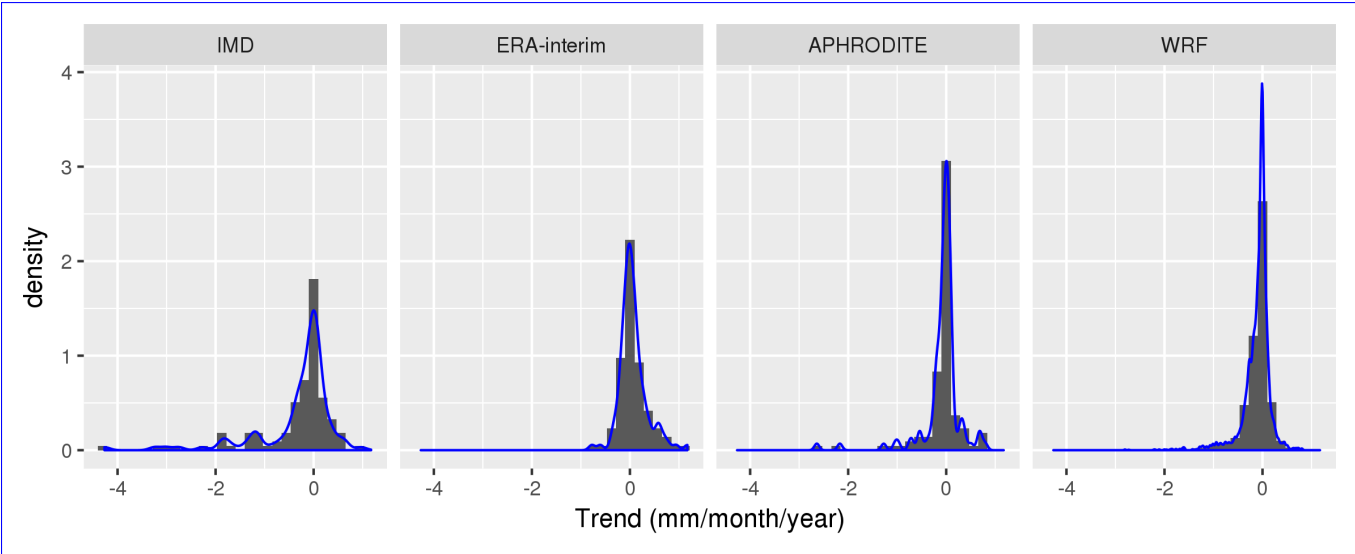
Figure 11. Trend (mm/month/year) of winter precipitation.
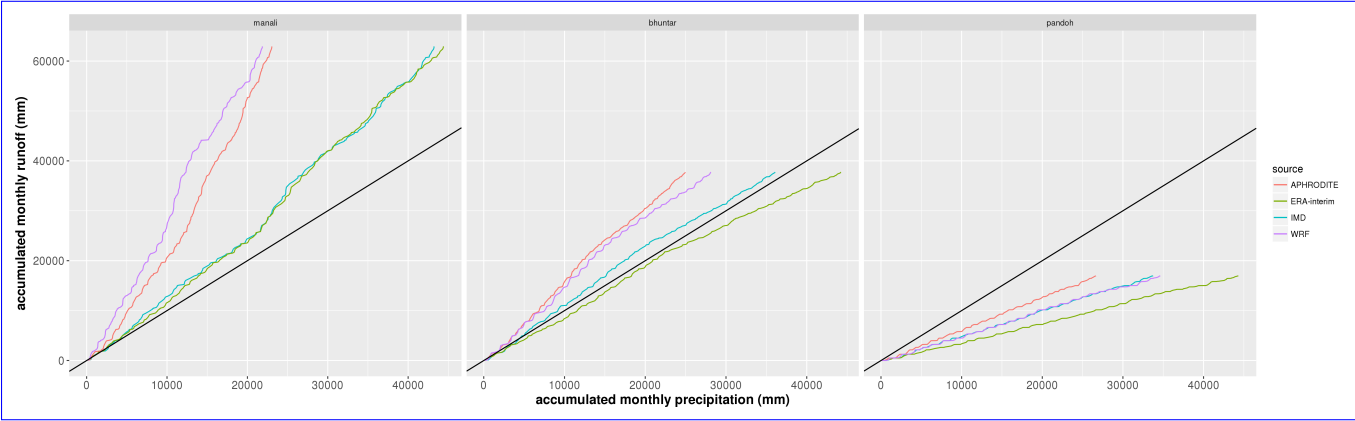
Figure 12. Accumulated monthly precipitation and discharge.

Figure 13. Mean temperature and its regression lines for the periods of 1981-1985 and 2003-2007 by the WRF simulation.

Tables

Table 1. Summary of weaknesses of four types of gridded precipitation data.

Data type	Weaknesses
Satellite	Dependence on platforms and sensors; bias caused by snow and ice
Interpolations	Inadequacy of interpolating methods; unavoidable inferiors inherited from gauge measurements
Output from climate models	Inadequacy in algorithms, boundary and forcing
Reanalysis	changes in observation system; model error

Table 2. The main settings of the WRF regional climate model. The complete setting are shown in supplementary file.

Time and Domain	
Period	1979-2007
Region	59-91E, 9-46N
Horizontal grid spacing	16,306 km
Dimension	(193, 241, 38)
Model top pressure	50 hPa
Physics	
Microphysics	Thompson scheme
Shortwave radiation	CAM
Longwave radiation	CAM
Surface-layer	Monin-Obukhov (Janjic) scheme
Land surface	Noah Land-Surface Mode
Boundary-layer	Mellor-Yamada-Janjic TKE scheme
Cumulus	Kain-Fritsch (new Eta) scheme
Lateral boundaries	
Forcing	ERA-Interim $0.75° \times 0.75°$, 6 hourly

Table 3. Pearson's correlation of annual precipitation series

Data \ Data	IMD	ERA-interim	APHRODITE	WRF
IMD	-	0.86	0.91	*0.64*
ERA-interim	0.86	-	0.86	*0.64*
APHRODITE	0.91	0.86	-	*0.59*
WRF	*0.64*	*0.54*	*0.59*	-

Appendix A: Appendix
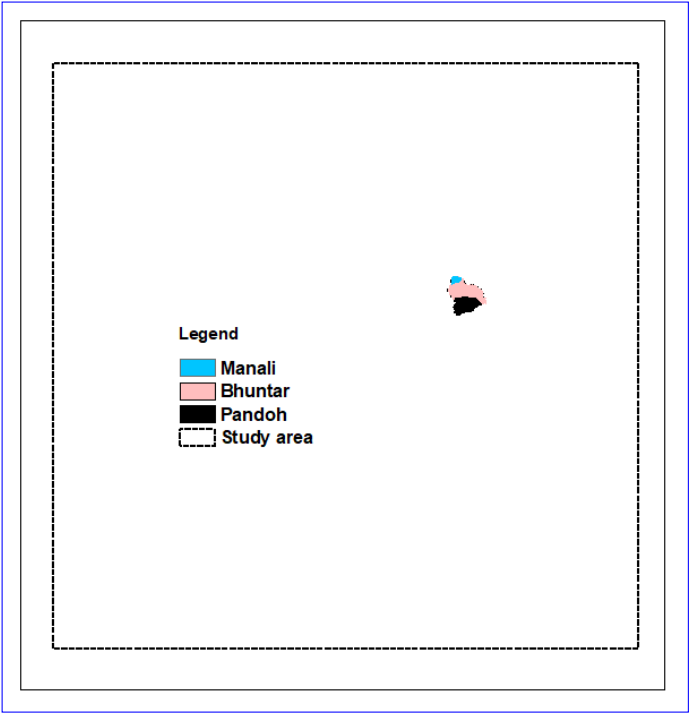
Figure A1. Locations of selected catchments.